ROBUST FEATURE EXTRACTION POSE ESTIMATION DURING FLY-AROUND AND STRAIGHT-LINE APPROACH IN CLOSE RANGE

K. Klionovska, M. Burri, and H. Frei

German Aerospace Center (DLR)/German Space Operations Center (GSOC), 82234 Weßling, Germany,
ksenia.klionovska@dlr.de,matthias.burri@dlr.de, heike.frei@dlr.de

ABSTRACT

This paper refers to the field of visual navigation in On-Orbit Servicing (OOS) and/or Active Debris Removal (ADR) missions. Mainly the robust feature extraction pose estimation technique is proposed here to estimate target while approaching it. This method is tested with two image datasets from different sensors in open loop. The stable tracking during the fly-around and straight line approach gives a positive feedback to consider this technique as a possible candidate for the future missions.

Key words: On-Orbit Servicing, pose estimation, rendezvous.

1. INTRODUCTION

Technological process in the field of space robotics for future On-Orbit Servicing (OOS) and Active Debris Removal (ADR) missions goes ahead. Different companies and space agencies are developing sophisticated mission concepts for in-orbit maintenance of the satellite or deorbiting of no more functional space objects. One of the research activities in our group at DLR directs to the autonomous rendezvous towards a non-cooperative target (without orbital control system) with active or passive visual sensors.

Usually different optical sensors, mainly cameras and lidars, are used for automated rendezvous. Cameras, in its turn, also have different optics for narrow field of view (NFOV) and wide field of view (WFOV). In Mission Extension Vehicles (MEV) built by Northrop Grumman the Visible Sensor System (VSS) has 2 NFOV sensors for long range tracking and 2 WFOV close range tracking cameras (Pyrak & Anderson, 2021). In ATV mission the Service Module camera had two selectable FOVs: narrow angle 13°50'x10°20' and wide angle 64°x50° (De Rosa & Curti, 2006). LICIACube - the Light Italian Cubesat for Imaging of Asteroids (part of a NASA Double Asteroid The Redirection Test (DART) mission launched in November 2021) is equipped with two optical cameras. There are a NFOV panchromatic camera to acquire images from long distance with a high spatial resolution and a WFOV RGB camera, allowing a multicolor analysis of the asteroidal environment (ASI, 2021). In this work we use two optical cameras with different lenses for narrow and wide field of views. The NFOV sensor keeps the sufficintly large part of FOV with a target at longer ranges. The camera with WFOV, on the other hand, allows to retain the geometry of the target in closer ranges near the mating point.

The Robust Feature Extraction (RFE) pose estimation (PE) is a concept proposed in this paper for estimation of relative pose of the space object with images taken with NFOV and WFOV cameras. The idea of RFE PE appeared while reading the following paper Capuano et al. (2019). The working principle of RFE PE will be described in details in the next Section. Within this paper we are going to answer two questions. First, if the proposed pose estimation technique is suitable for both cameras and a stable tracking. Second, how much effort it takes to adjust the parameters of the RFE PE to the whole operation range. To answer these questions we setup a maneuver with the European Proximity Operation Simulator (EPOS) (Rems et al., 2021). The test data images with both cameras and also a ground truth were collected during straight-line approach and fly-around.

2. MATERIALS AND METHODS

2.1. EPOS and Cameras

EPOS 2.0 is a Hardware in the Loop (HIL) simulator for spacecraft rendezvous maneuvers. One industrial robot with visual sensors is able to move on the linear rail simulating the chaser, the other one (simulates target) carries a true scale mockup and fixed in the laboratory hall. The strong light spot is used also during rendezvous simulations to replace a real sunlight. In Figure 1 the sketch of EPOS is presented. The angle α on the image presents the changes of azimuth. The characteristircs of two visual cameras used in this paper are presented in Table 1.

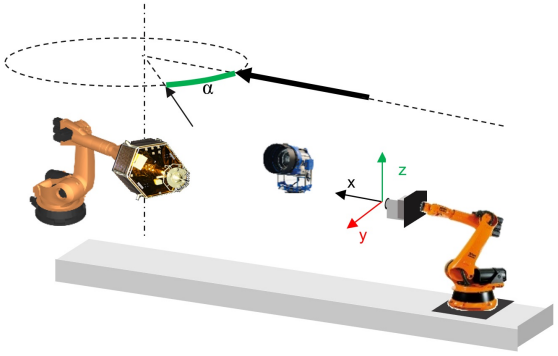

Figure 1: Graphical presentation of the test setup at EPOS.

Table 1: Cameras characteristics

Name	NFOV	WFOV
Model	Prosilica GT205 (02-2626A)	
Pixel size [μm]	5.5 x 5.5	
Sensor field [pixel]	2048 x 2048	
Focal length [mm]	35.0	12.5
FOV [°]	18 x 18	47 x 47

2.2. Robust Feature Extraction and Pose Estimation

The consequent steps needed for relative pose estimation are given in Figure 2.

Figure 2: Consequent steps to get a relative pose.

The gray/scaled image is obtained from a monocular camera. Thereafter multiple features are extracted from this input image. We extract end points of lines using the Hough Line Transform (HLT) algorithm (Hough, 1962) and corners using Shi-Tomasi (ST) (Shi & Tomasi, 1994) algorithm. These algorithms will be described in following subsections 2.2.1-2.2.2. As a result of HLT and ST, we have a large set of 2D image points from two sources. For calculation of the pose, we assume in this work that the 3D geometrical model of the target object is known. In the feature matching box of Figure 2, the matches between projected model points and set of image points are identified using a 2D space neighbour search. Finally, an efficient perspective-n-point (Epnp) solver (Lepetit et al., 2008) is used to estimate the pose of the target. The open source OpenCv library (Bradski, 2000) is used for some parts of RFE PE.

2.2.1. Hough Line Transform

Probabilistic Hough Line Transform (Matas et al., 2000) is an efficient method for line detection with binary images, which was introduced some years ago. We used *HoughLinesP* function from the OpenCv library for getting appropriate set of image lines. This function has multiple input parameters: distance resolution of the accumulator in pixel, angle resolution of the accumulator in radians, an accumulator threshold parameter, minimum line length, and maximum line gap. The size of accumulator for lines search is equal 2. The tuning of these parameters is a very challenging part of HLT. We have properly faced this problem using two cameras with different FOVs. In Figure 4 there are two images taken at the same distance during simulation with azimuth 50 deg. The lines found with this method in the images of NFOV and WFOV cameras in Figure 3 are obviously different. For example, the upper line of hexagone contour in image 3a is correctly found and not broken. In image 3b only some parts of the straight line are detected. It confrms the need for accurate selection of parameters during the testing phase of the algorithm.

2.2.2. Shi-Tomasi Corners Detection

Shi-Tomasi corners detection is almost similar version of the Harris detector (Harris & Stephens, 1988). The difference of ST corner detection is in score calculation. Score is calculated for every pixel, and if the score is above a certain value, this pixel is accepted as a corner. Moreover, the ST function provides only N most strong corners from all defined. In OpenCv library this function is called *goodFeaturesToTrack()*, where some input parameters should be tuned manually.

3. RESULTS

This section provides the maneuver details, see Table 2, and the numerical assesment of the pose errors after open loop tests. During frontal approach and fly-around different images with both cameras as well as a ground truth were collected.

Table 2: Maneuver details

Maneuver	Duration [s]	Sensor
Frontal Approach 12m – 10m	143.3	NFOV
Fly-Around Azimuth 90°- 45°	299.3	NFOV
Fly-Around Azimuth 40°- 90°	339.3	WFOV
Frontal Retreat 10m – 12m	140.7	WFOV

There were no sophisticated filter used for object prediction or noise reduction during the post processing open

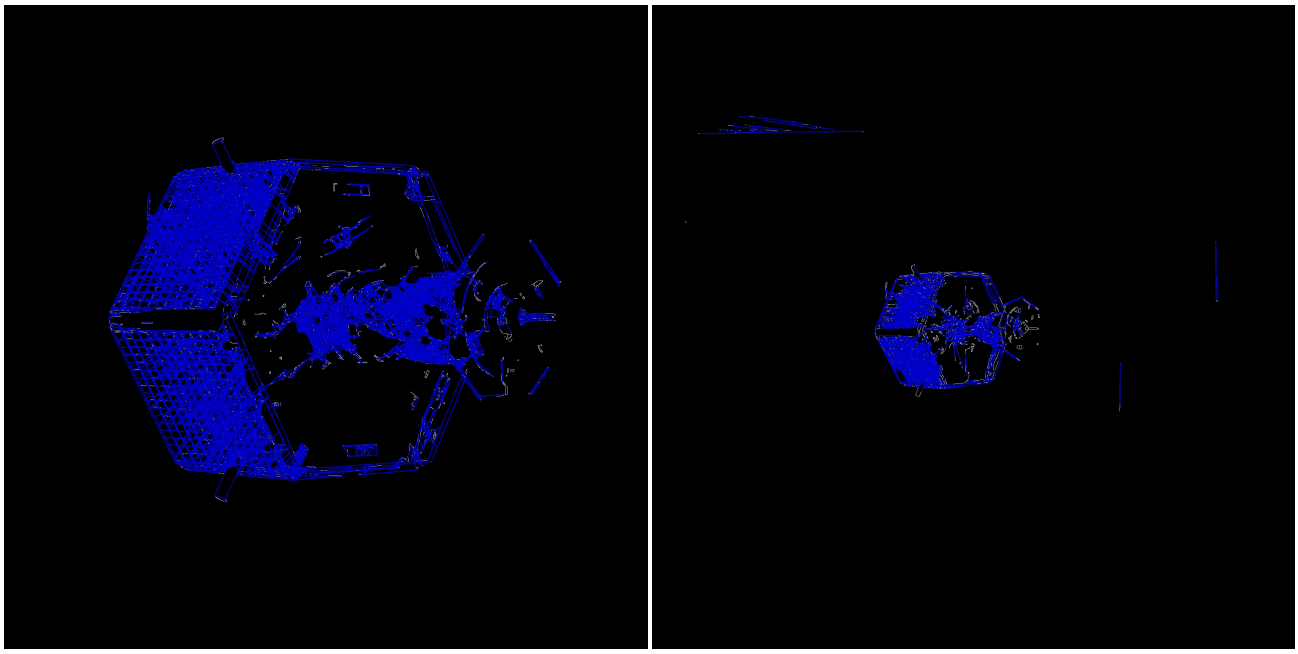

(a) NFOV camera image (b) WFOV camera image

Figure 3: Hough Lines in blue in (3a) of NFOV and in (3b) of WFOV

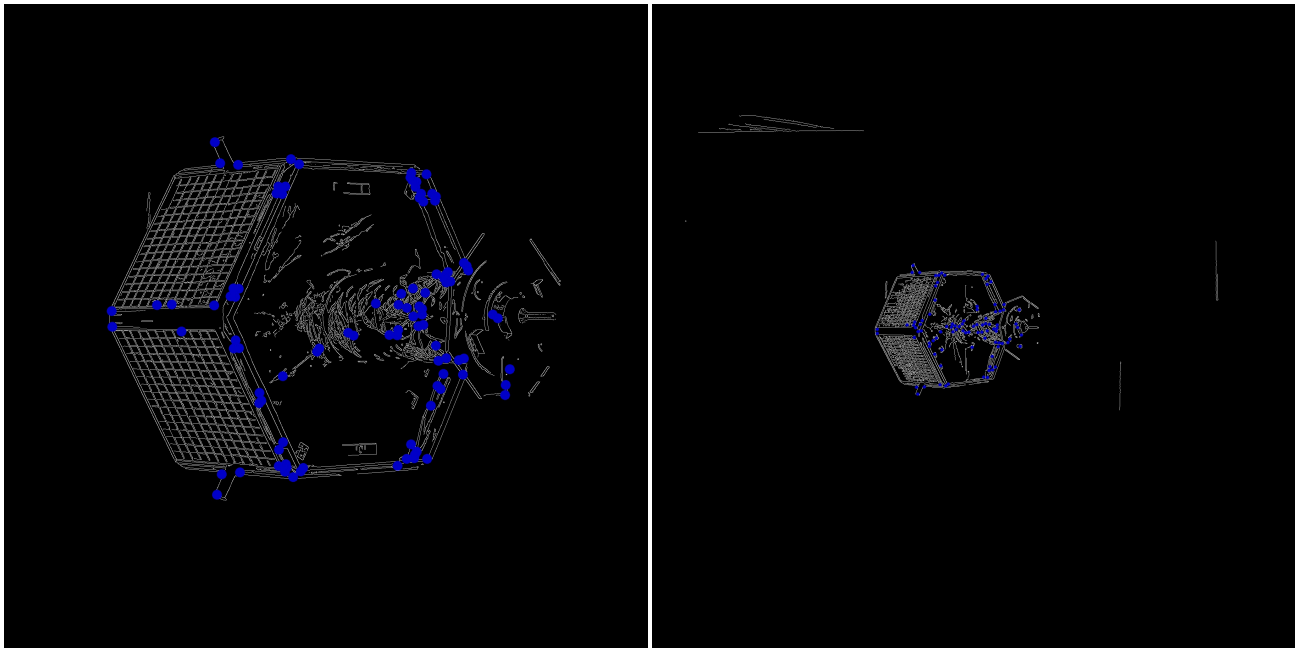

(a) NFOV camera image (b) WFOV camera image

Figure 4: Shi-Tomasi corners in blue in (4a) of NFOV and in (4b) of WFOV

loop tests. At the beginning the tracker was intialised with a reference pose with some noise. In the subsequent images the estimated pose with the previous image was used as a guess for the next one. We should not exclude the fact, that after some tracker failure the real pose can quickly diverge because of accumulated errors.

We have conducted the open loop test with the proposed pose estimation technique and images from NFOV sensor. The good input parameters for HLT and ST used for the results presented below in Table 3. Figure 5 and Figure 6 present estimated errors of position and orientation for the frontal approach from 12 to 10 meters and fly-around. This is just a first example approach with such sensors. Approaches with larger ranges are planned to be done in the near future. Therafter we have run the al-

gorithm with the dataset of images from WFOV camera. Figure 7 and Figure 8 present estimated errors of position and orientation for fly-around and straight retreat back to 12 m. The open loop tracking were successful in both cases. The pose could be estimated for every image.

Table 3: HLT and ST input parameters

HLT input parameters	**NFOW**	**WFOW**
distance resolution [pixel]	0.5	1
angle resolution [°]	1.0	0.29
accumulator threshold [-]	10	20
min line length [pixel]	50	40
max line gap [pixel]	10	5
ST input parameters		
free coefficient [-]	0.05	0.05
sobel aperture [pixel]	3	3
quality level [-]	0.01	0.01
max corners [-]	100	100
min distance [pixel]	10	5

Let us discuss estimated pose errors for NFOV camera. The position error along X axis in Figure 5 has reached its maximum 0.6 m during the fly-around. During the straight line approach around timestamp 50 sec the estimated position error was around 0.41 m. The position errors along Y and Z axes are small and not higher than 0.15 m. For the estimation of the orientation error we use an angular difference between two quaternions - the ground truth orientation and estimated one. In Figure 6 one can observe the maximum angular error around 6 deg during the fly-around at the end of simulation, ca. 3 deg error during the frontal approach. The position error along X axis for WFOV sensor was 4 times a bit more than 0.6 m during the fly-around and straight-line approach. At the begginning of the straight line retreat the position error along X axis was less than 0.2 m at a timestamp 345 sec. With the distance increase between the chaser and target, the error started also to become higher and reached again 0.6 m at the end. The position errors along other two axes were not higher than 0.15 m during the whole tracking with WFOV sensor. The angular error reached 6.5 deg during the fly-around and thereafter is not higher than 5 deg.

Some of images with calculated pose in purple during the tracking are presented in Figure 9 for NFOV camera and in Figure 10 for WFOV camera.

4. DISCUSSION AND CONCLUSION

This paper provides a description of the proposed robust feature extraction technqiue for pose estimation. The functionlity of the RFE PE is presented with open loop tests conducted with NFOV and WFOV cameras. In both simulations the frontal and side tracking of the target mockup was successful and the pose esimation error is acceptable. The algorithm could cope even with some jumps in estimated pose, thus the error could be compensated on its own and without any external influence. It should be noted, that in the results section we present only one test case per camera dataset. It took us a time to sort out parameters of HLT and ST presented in Table 3, do open loop tests and analyse the errrors, before we got a positive output. This appeared to be a challenging part in this research. The RFE PE has been already integrated in our GNC system. The further step of this research is harware-in-the-loop simulations with both sensors and proposed RFE PE technqiue.

REFERENCES

ASI. 2021, Light Italian Cubesat for Imaging of Asteroids

Bradski, G. 2000, Dr. Dobb's Journal of Software Tools

Capuano, V., Alimo, S. R., Ho, A. Q., & Chung, S.-J. 2019

De Rosa, D. & Curti, F. 2006, in 6th International ESA Conference on Guidance, Navigation and Control Systems

Harris, C. & Stephens, M. 1988, in Proceedings of the 4th Alvey Vision Conference, 147–151

Hough, P. V. 1962

Lepetit, V., Moreno-Noguer, F., & Fua, P. 2008, International Journal of Computer Vision, 81, 155

Matas, J., Galambos, C., & Kittler, J. 2000, Comput. Vis. Image Underst., 78, 119–137

Pyrak, M. & Anderson, J. 2021, in 2021 AMOS Conference, Maoui, Hawai, 19 Oct 2021

Rems, F., Frei, H., Risse, E.-A., & Burri, M. 2021, Aerospace, 8

Shi, J. & Tomasi. 1994, in 1994 Proceedings of IEEE Conference on Computer Vision and Pattern Recognition, 593–600

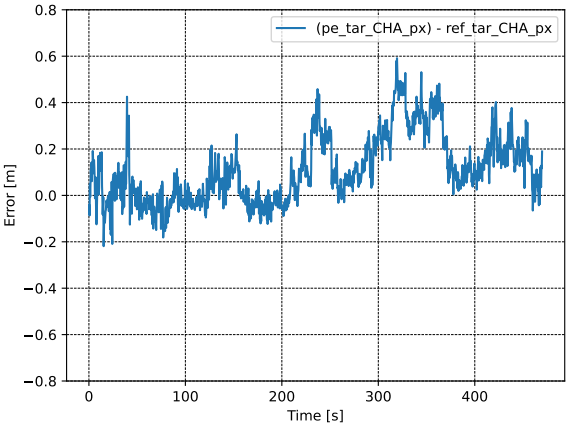

(a) Pose estimation errors X axis

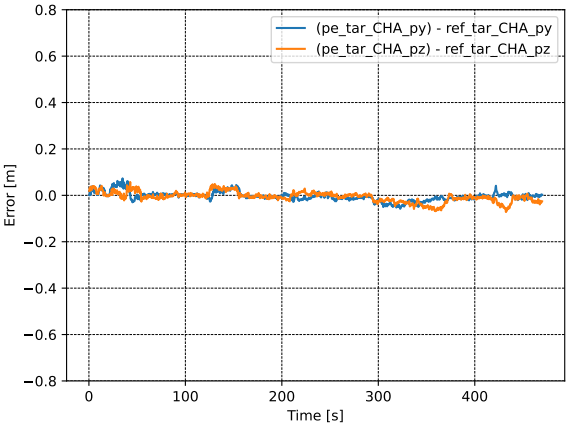

(b) Pose estimation errors Y and Z axes

Figure 5: Calculated position errors during maneuver with NFOV camera.

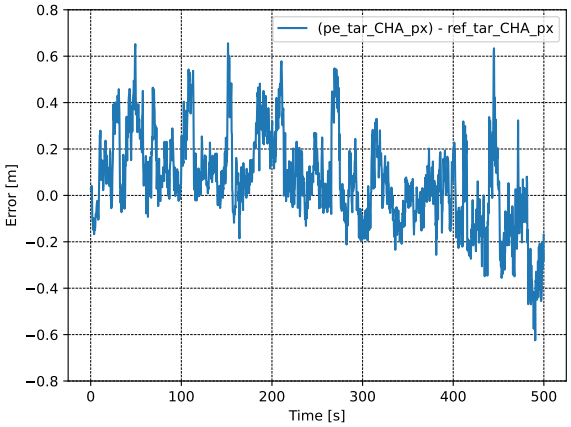

(a) Pose estimation errors X axis

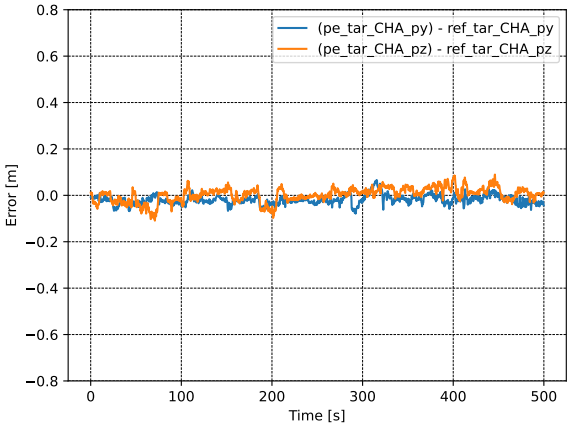

(b) Pose estimation errors Y and Z axes

Figure 7: Calculated position errors during maneuver with WFOV camera.

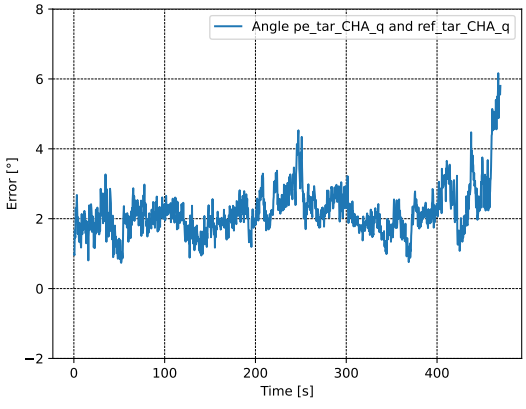

Figure 6: Calculated attitude error during maneuver with NFOV camera.

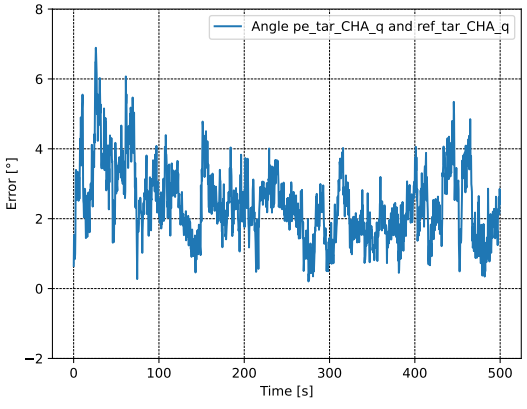

Figure 8: Calculated attitude error during maneuver with WFOV camera.

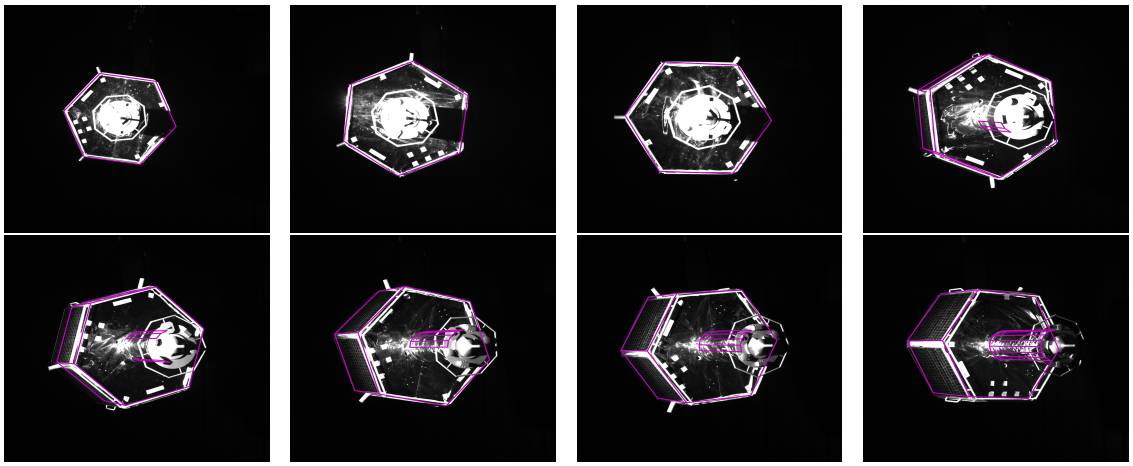

Figure 9: Images of NFOV camera with estimated pose during straight line approach and fly-around.

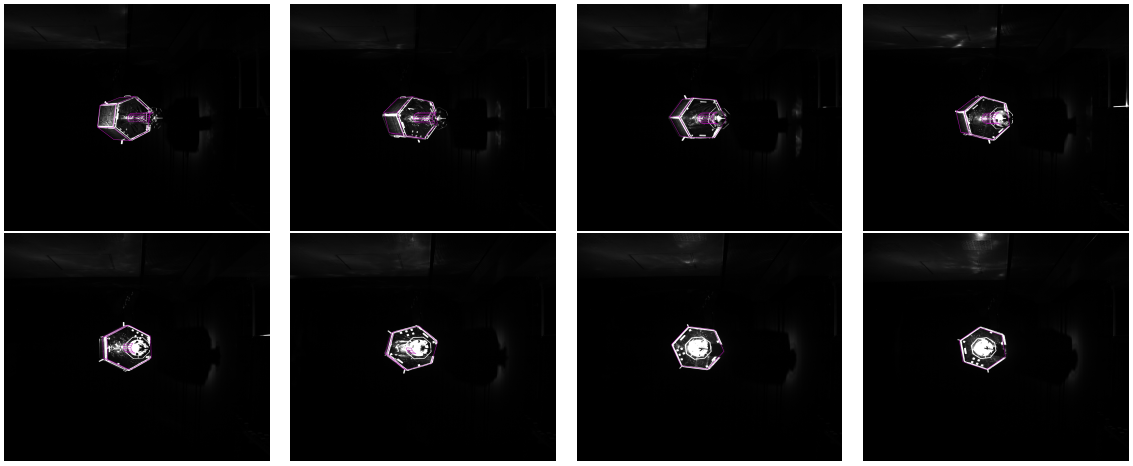

Figure 10: Images of WFOV camera with estimated pose during straight line approach and fly-around.